ACCOUNTS of chemical research

Article

pubs.acs.org/accounts

Density Functional Theory Modeling of Multilayer "Epitaxial" Graphene Oxide

Si Zhou and Angelo Bongiorno*

School of Physics, School of Chemistry and Biochemistry, Georgia Institute of Technology, Atlanta, Georgia 30332, United States

CONSPECTUS: Graphene oxide (GO) is a complex material of both fundamental and applied interest. Elucidating the structure of GO is crucial to achieve control over its properties and technological applications. GO is a nonstoichiometric and hygroscopic material with a lamellar structure, and its physical chemical properties depend critically on synthesis procedures and postsynthesis treatments. Numerous efforts are in place to both understand and exploit this versatile layered carbon material.

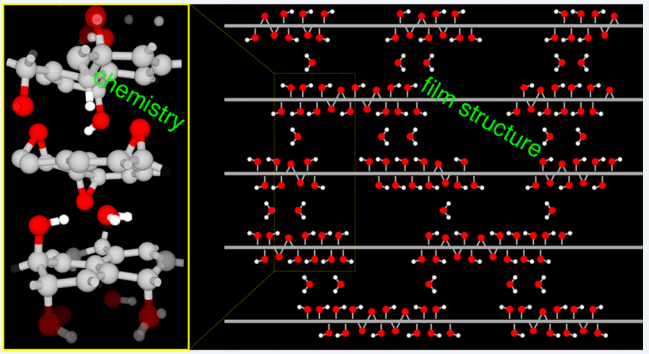

This Account reports on recent density functional theory (DFT) studies of "epitaxial" graphene oxide (hereafter EGO), a type of GO obtained by oxidation of graphene films grown epitaxially on silicon carbide. Here, we rely on selected X-ray photoelectron spectroscopy (XPS), infrared spectroscopy (IR), and X-ray diffraction (XRD) measurements of EGO, and we discuss in great detail how we utilized DFT-based techniques to project out from the experimental data basic atomistic information about the chemistry and structure of these films. This Account provides an example as to how DFT modeling can be used to elucidate complex materials such as GO from a limited set of experimental information.

EGO exhibits a uniform layered structure, consisting of a stack of graphene planes hosting predominantly epoxide and hydroxyl groups, and water molecules intercalated between the oxidized carbon layers. Here, we first focus on XPS measurements of EGO, and we use DFT to generate realistic model structures, calculate core-level chemical shifts, and through the comparison with experiment, gain insight on the chemical composition and metastability characteristics of EGO. DFT calculations are then used to devise a simplistic but accurate simulation scheme to study thermodynamic and kinetic stability and to predict the intralayer structure of EGO films aged at room temperature. Our simulations show that aged EGO encompasses layers with nanosized oxidized domains presenting a high concentration of oxygen functionalities and local structural order, surrounded by regions of pristine graphene. Through the analysis of XRD and IR measurements, our DFT calculations finally show that in EGO, the oxidized domains of stacked layers overlap and locally confine about a monolayer of water molecules. The overall water content in EGO remains below 10%, and intralayer and interlayer spatial ditribution of oxygen species in EGO lead to a layered porous film with an interlayer spacing of about 10 Å.

The basic insight gained from our DFT studies, from chemical composition to a nanoscale characterization of the film structure, will be used to fine-tune synthesis methods and EGO properties.

1. INTRODUCTION

Graphene oxide (GO) is a layered material with intriguing physical chemical properties[1] and a variety of potential applications.[2−7] Synthesized for the first time in 1859,[8] today GO is commonly obtained by oxidation of graphite via the Hummers or equivalent methods,[9−11] followed by several solution processing steps.[9−11] This type of GO consists of a disorganized stack of oxidized graphene platelets.[12−14] The oxidized carbon sheets encompass aromatic areas with unoxidized benzene rings, regions containing aliphatic six-member rings hosting mostly epoxide and hydroxyl groups, and at the edges of the platelets, oxygen functional groups such as carbonyl and carboxyl groups.[15,16] Oxygen functionalities bonded to the carbon layers are present in concentrations and relative fractions depending on both synthesis and postsynthesis treatments, and since GO is a hygroscopic material, water molecules can also incorporate in the lamellar structure.[16−19]

In recent years, GO has been the focus of numerous experimental and computational studies. Most of the recent experimental efforts have focused on improving the synthesis method,[10,11] exploring alternative routes to obtain new forms of GO,[20,21] optimizing GO applications such as optoelectronics or catalysis,[22,23] and studying and characterizing at a fundamental level the physical and chemical properties of both as-synthesized and thermally or chemically treated GO materials.[21,24−26] In less than a decade of experimental work, much progress has been made in all these directions. A most recent

Special Issue: DFT Elucidation of Materials Properties

Received: December 9, 2013
Published: May 20, 2014

   dx.doi.org/10.1021/ar400288h | Acc. Chem. Res. 2014, 47, 3331−3339

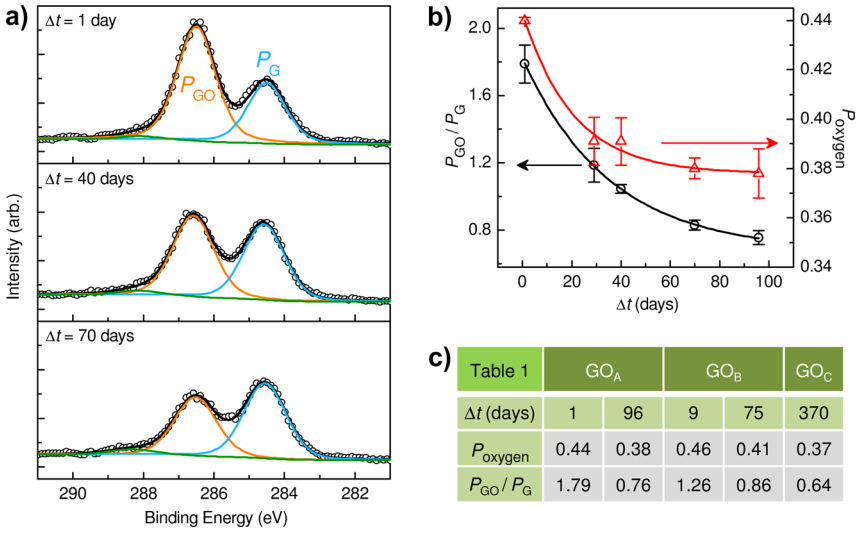

c)

Table 1	GO_A		GO_B		GO_C
Δt (days)	1	96	9	75	370
P_{oxygen}	0.44	0.38	0.46	0.41	0.37
P_{GO}/P_G	1.79	0.76	1.26	0.86	0.64

Figure 1. (a) C_{1s} XPS spectra of a EGO film. Open circles show experimental data. The black lines show the fitting curves. (b) P_{GO}/P_G (black) and O/C (red) ratios obtained from spectral analyses; symbols show mean values and errors derived by analyzing XPS spectra acquired from different regions of the EGO film. The solid lines show exponential fits. (c) Table reporting oxygen content and P_{GO}/P_G ratios vs aging time of three different EGO films.

experimental accomplishment in this area is the discovery of the anomalous water and ion permeation properties of GO.[27−29] This discovery opens new application opportunities of GO in filtration and separation, along with new questions and challenges for both the experimental and computational chemistry communities.

Recent computational studies of GO have led to detailed information about this complex material.[30−32] Density functional theory (DFT) calculations have been used so far to address questions such as the relationships between chemistry, structure, and electronic properties of GO,[33−39] its chemical stability,[26,35,40−43] the nature of oxidation and reduction mechanisms of graphene layers,[44−50] vibrational, optical, and core level spectroscopy, and nuclear magnetic resonance spectroscopy signatures of GO,[4,26,51,52] and the effect of water content on the interlayer structure and mechanical properties of multilayer GO.[7,43] Current and future challenges for DFT include modeling and studying realistic GO materials, elucidating the mechanisms responsible for the conversion during the synthesis process of graphene or graphite to GO, explaining surprising behaviors such as its permeability properties,[53] and clarifying how ambient conditions, single- vs multilayer geometry, and substrate materials influence chemistry, structure, and properties of GO. In this Account, we report on our recent computational effort to elucidate the structure of GO films obtained by chemical oxidation of multilayer epitaxial graphene (EG) grown on a SiC substrate.[25,26,40,54] To avoid confusion and highlight the nature these films, hereafter we will refer to this type of GO obtained from EG as EGO.

The DFT scheme[55] employed in the studies[25,26,40,54] here discussed is based on the use of the supercell geometry, plane wave basis sets, norm-conserving pseudopotentials, the generalized gradient approximation for the exchange and correlation energy functional proposed by Perdew, Burke, and Ernzerhof,[56] and semiempirical corrections to account for dispersion forces.[57] In the following sections, we will show how we utilized our standard DFT approach to project out from a limited set of experimental data basic information about the chemistry and the structure of EGO.

2. SYNTHESIS OF EGO

Chemical oxidation of multilayer EG grown on the C-face of a SiC substrate is carried out by the Hummers method.[9] This method employs a mixture of sodium nitride, a concentrated solution of sulfuric acid, and potassium permanganate as oxidizing agent. Oxidation of EG occurs in an iced bath, it lasts approximately 30 min, and it is terminated by adding deionized water and hydrogen peroxide to the mixture. Modeling from *first-principles* the oxidation mechanisms occurring during the chemical synthesis of EGO is a formidable task. Here, our DFT studies are focused on elucidating the structural and chemical properties of EGO films that are held at room temperature in standard ambient conditions after the synthesis process.

3. CHEMICAL COMPOSITION OF EGO

Figure 1a shows C_{1s} X-ray photoelectron spectroscopy (XPS) spectra of an EGO film taken at different aging times.[26,54] These spectra show the occurrence of three main peaks: a peak P_G arising mainly from sp^2 C atoms, a peak P_{GO} attributed to epoxide and hydroxyl groups, and a peak at higher binding energies associated with carbonyl species. The small area of this latter peak shows that EGO contains small amounts of carbonyl species, while the absence of peaks at binding energies higher than 289 eV shows that EGO consists of a stack of large-area graphene oxide sheets presenting a negligible quantity of edge groups such as carboxyl species.[26,54] The XPS spectra show also that, at room temperature, the structure and chemistry of EGO change significantly over a period of several weeks after the synthesis process. The O/C ratio ("P_{oxygen}" in Figure 1b) decreases from 0.44 in as-synthesized EGO to 0.38 after aging the films at room temperature for more than 2 months. Over the same period of time, the P_{GO}/P_G ratio, which corresponds to a measure of the number of C−O bonds in EGO, drops from 1.79 to about 0.76 (see also table in Figure 1c).

To analyze from *first-principles* the experimental XPS spectra shown in Figure 1, we used our DFT scheme to calculate XPS

dx.doi.org/10.1021/ar400288h | Acc. Chem. Res. 2014, 47, 3331−3339

spectra of realistic model structures of EGO including a fixed O/C ratio and selected fractions of epoxide, hydroxyl, and water molecule species (Figure 2).[26,54] In the case of as-

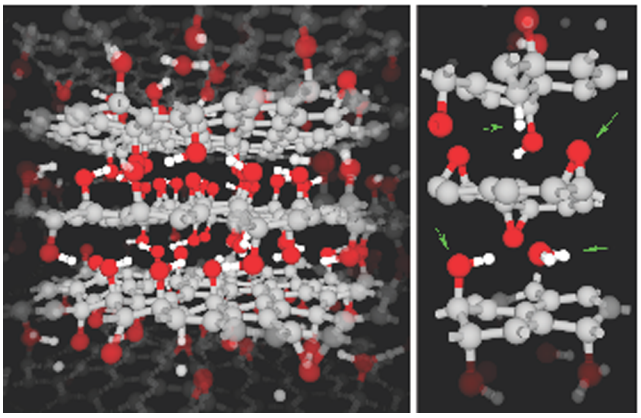

Figure 2. (left) Model structure of EGO generated from DFT. (right) Selected region of the same model showing the predominant chemical species present in EGO; clockwise from the top and indicated by the green arrows: C−H, epoxide, water, and hydroxyl species. Gray, red, and white colors are used to represent C, O and H atoms, respectively.

synthesized EGO, we found that the model structures with O/C = 0.44 yielding the best agreement with the experiment are those devoid of water molecules and incorporating about 26% and 18% (percentages are relative to total amount of C) of epoxide and hydroxyl species, respectively (Figure 3). Additional comparisons with the experiment demonstrated that this optimal chemical composition satisfies two important requirements. First, it leads to calculated XPS spectra whose P_{GO}/P_G ratio is in excellent agreement with the experiment. Second, it leads to oxidations of the graphene planes poor in ethers and doubly oxidized C species (Figure 3). EGO models incorporating more than 2% of water molecules violate either or both these requirements, leading to XPS spectra in disagreement with the experiment (Figure 3).

Aged EGO loses 15% of the initial amount of oxygen and yields the XPS spectra shown in Figure 1. Our DFT analysis showed that a range of chemical compositions of aged EGO is consistent with the experiment (Figure 4). In particular, we found that at O/C = 0.38 and for any water content up to 8%, it is possible to generate a model structure of aged EGO incorporating optimal fractions of epoxide and hydroxyl species to yield an XPS spectrum in satisfactory agreement with the experiment (Figure 4). Interestingly, all the acceptable chemical compositions of aged EGO had something in common: the total amount of hydrogen is larger than 18%, the percentage of hydrogen present in the form of hydroxyl species in as-synthesized EGO.

Overall, our DFT analysis of the XPS spectra of EGO leads to two important conclusions. First, the amount of water in the EGO films appears to increase over time. Second, as-synthesized EGO incorporates an excess quantity of hydrogen, not in the form of water or hydroxyl species. We can explain both these results and the changes of the XPS spectra observed experimentally using simple chemical arguments. Chemical oxidation of EG occurs in an acid solution and involves washing steps. It is therefore very likely that not only oxygen but also hydrogen incorporates into the films and chemisorbs on graphene layers, leading to the formation of C−H species.

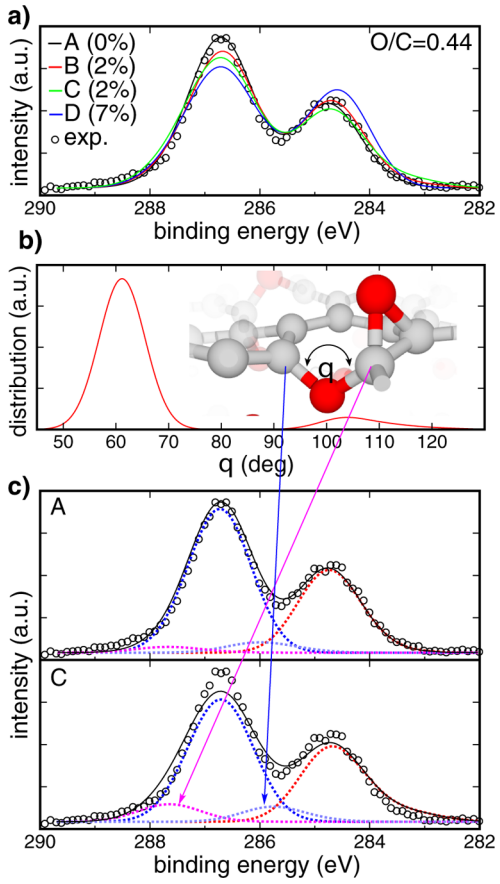

Figure 3. (a) Experimental (circles) and calculated (solid lines) C_{1s} XPS spectra of as-synthesized EGO. Percentages in parentheses refer to the water content in the models. (b) C−O−C bond angle distribution in epoxide and ether species present in the model structures of EGO generated from DFT. The distribution shows that epoxide and ether groups are both geometrically and chemically (i.e., C_{1s} core-level binding energies) different. (c) C_{1s} XPS spectra obtained from DFT by using models A and C. Open circles show the experimental data. The computed spectra are decomposed in four peaks: sp^2 C atoms (red dashed line), C atoms in epoxide or hydroxyl species (blue dashed line), ether groups (light-blue dashed line), and doubly oxidized C atoms (pink dashed line).

Model	H_2O	epoxides	hydroxyls
E	0.01	0.10	0.27
F	0.08	0.25	0.05
G	0.00	0.18	0.20

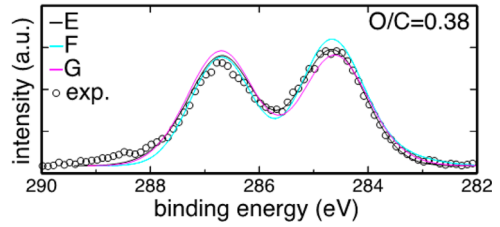

Figure 4. (top) Table reporting the chemical composition of the model structures of aged (70-days) EGO used to interpret the experimental data (bottom). Experimental (circles) vs calculated (solid lines) C_{1s} XPS spectra of an EGO film aged for 70 days at room temperature.

dx.doi.org/10.1021/ar400288h | Acc. Chem. Res. 2014, 47, 3331−3339

These species react readily with epoxide and hydroxyl groups, and these reactions may be at the origin of the observed metastability characteristics of EGO. This picture was corroborated by a list of DFT calculations (Figure 5), and the presence of C−H in GO was also confirmed by infrared spectroscopy.[26,58,59]

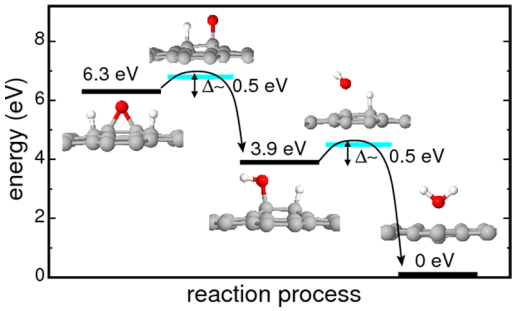

Figure 5. Energies involved in the reactions of C−H species with, first, an epoxide group and, second, a hydroxyl species on graphene. Black segments show the energy of isolated species on graphene: (left) two C−H species and one epoxide, (middle) one C−H and one hydroxyl species, and (right) a water molecule. Colored segments show the reaction energy barriers involved in the reactions.

4. STABILITY AND INTRALAYER STRUCTURE OF EGO

At room temperature, GO reduction through the formation and release of CO, CO_2, or O_2 molecules is inefficient, and our DFT analysis of the XPS spectra of EGO suggests that, after the synthesis process, EGO attains an equilibrium state by internal forming and releasing of water.[26,58,59] At room temperature, these processes die off in about 4−8 weeks. Two simple questions arise by considering the aging process of EGO: Why and how do the chemical and structural changes of EGO arrest? And what is the structure of the aged EGO films?

Figure 6 shows several plausible binary reactions between epoxide and hydroxyl groups on a graphene layer leading to the formation of O_2 and H_2O molecules. These reaction energy diagrams were obtained by performing nudged elastic band (NEB)[40] DFT calculations of pairs of oxygen functionalities on graphene. Energy values of reagents and products in Figure 6 correspond to Gibbs free energies of formation per oxygen defect. This quantity was calculated by using as reference systems pristine graphene and gaseous O_2 and H_2O molecules in air at room temperature and standard pressure. Interestingly, the Gibbs free energies of formation of isolated epoxide and hydroxyl species on graphene are 1.1 and 1.6 eV, respectively. These energy values show that sparse oxygen functionalizations of graphene are unstable in air and thereby prone to decompose into O_2, H_2O, and pristine graphene via the mechanisms shown in Figure 6.

Figure 6 also shows the energy gained by bringing together two well-separated oxygen functionalities on graphene to form a dimer species. These results show that epoxide and hydroxyl species on graphene attract each other and tend to agglomerate. The attraction is largest for hydroxyls, and for an arbitrary binary complex, it is larger when the oxygen functionalities are chemisorbed on the opposite sides rather than the same side of a graphene layer. A full map of interaction (or association) energies of pairs of oxygen functional groups on graphene is shown in Figure 7.[40] These DFT results show that binary interactions decay to negligible values when the oxygen functionalities are separated by more than four C=C bonds, showing a nontrivial pattern at smaller distances. The full set of pairwise interaction energies shown in Figure 7 was used to construct a simple energy scheme to calculate, without the need for a DFT calculation, the Gibbs free energy of formation of an arbitrary epoxy/hydroxyl functionalization of graphene.[40] This energy scheme was fine-tuned to match a variety of DFT results and then used to generate realistic model structures of aged

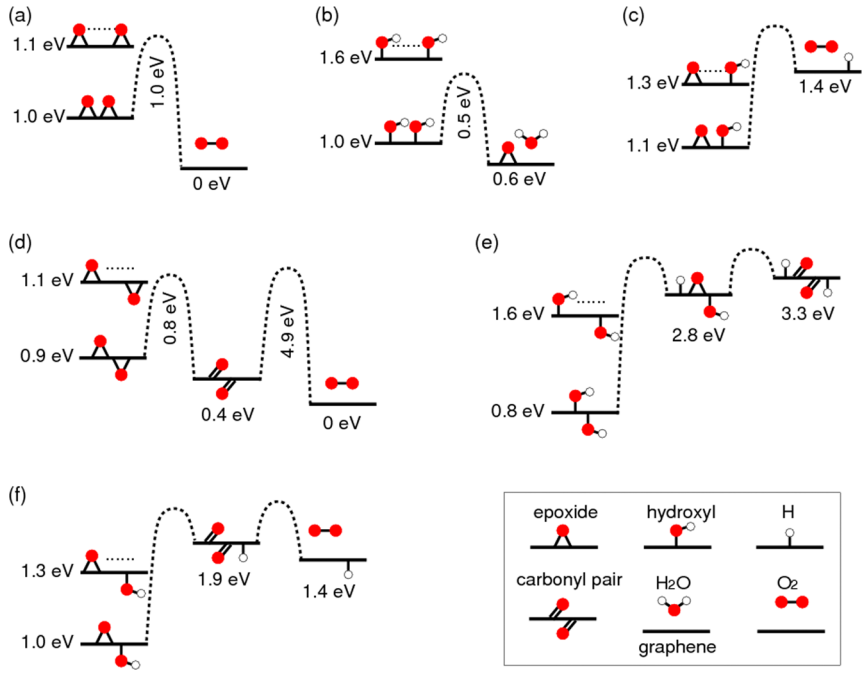

Figure 6. Binary decomposition reactions between epoxide and hydroxyl groups chemisorbed on either the same side or opposite sides of a single-layer graphene. The energy values correspond to Gibbs free energies of formation per oxygen species computed as described in the text.

dx.doi.org/10.1021/ar400288h | Acc. Chem. Res. 2014, 47, 3331−3339

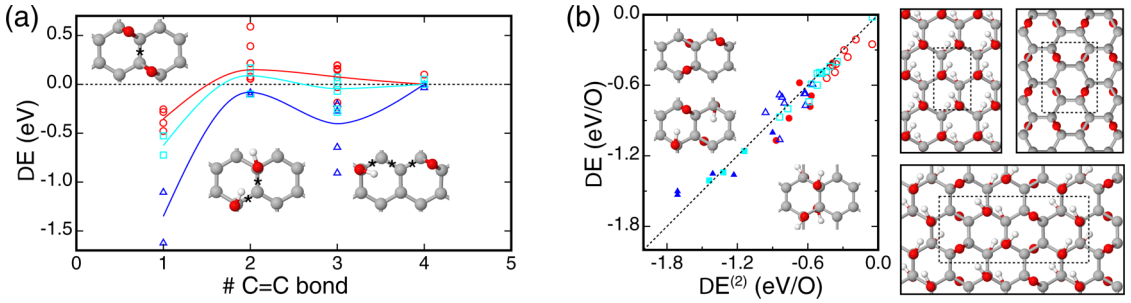

Figure 7. Association energy of pairs of oxygen functional groups on graphene: (a) epoxide−epoxide (red), hydroxyl−hydroxyl (blue), and epoxide−hydroxyl (cyan) binary complexes. Energy values are referred to the energies of pristine graphene and isolated species on graphene. Insets show selected binary complexes whose oxygen groups are separated by one, two, and three C═C bonds (asterisks). Solid colored lines are guides to the eye. (b) Energy values (per functional group) of single-layer EGO models presenting epoxy-only (red), hydroxyl-only (blue), and mixed epoxide−hydroxyl (cyan) functionalizations computed by using both DFT (ΔE) and the simplified energy scheme ($\Delta E^{(2)}$). Filled symbols refer to crystalline structures with high O/C ratios, while empty symbols show ΔE for sparse agglomerates of functional groups on graphene at low O/C ratios. Insets show selected EGO structures considered in the energy comparisons; C, O, and H are shown in gray, red, and white colors.

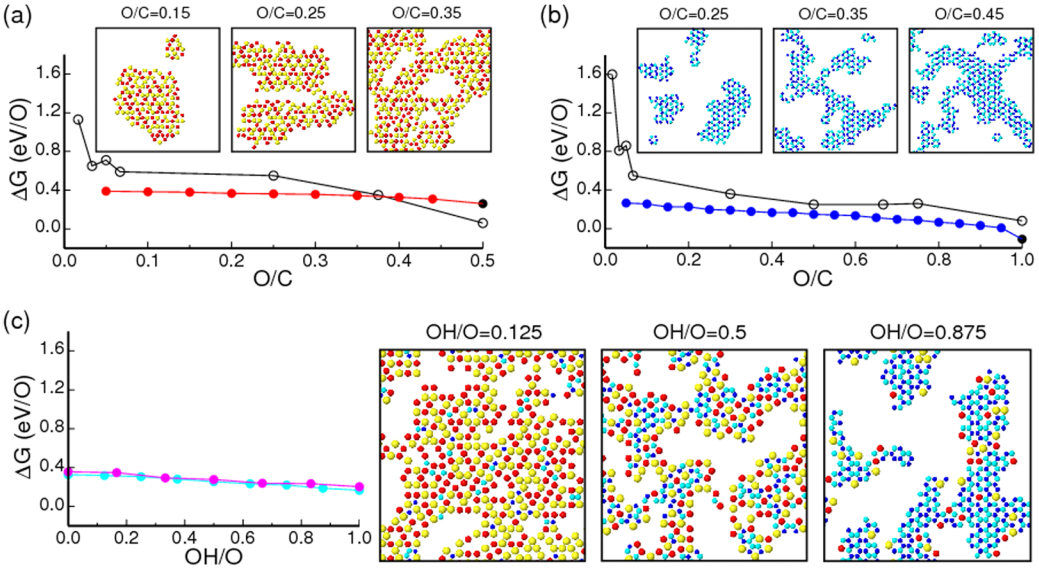

Figure 8. (a) Gibbs free energy of formation (ΔG) per oxygen functional group of EGO single-layers oxidized with only epoxide species. Black symbols show results obtained by using DFT and *handmade* model structures of EGO, while red symbols show the results obtained by using our simplified interaction energy scheme and Monte Carlo simulations. Insets show selected model structures of aged EGO functionalized with only epoxide groups: C atoms are not shown and red and yellow discs show epoxide groups facing upward and downward from the C basal plane, respectively. (b) Same as part a for the case of hydroxyl-only functionalizations of graphene. In the insets, hydroxyl species facing upward and downward from the carbon plane are shown in blue and cyan, respectively. (c) ΔG per functional group of EGO layers oxidized with both epoxide and hydroxyl groups. OH/O refers to the fraction of hydroxyl groups relative to the total amount of oxygen. The EGO models are generated via Monte Carlo simulations. Magenta and cyan symbols (connected by segments) refer to EGO models with fixed O/C ratios equal to 0.3 and 0.4, respectively. Illustrations on the right show selected configurations of aged EGO layers with an O/C ratio of 0.4 and different relative fractions of hydroxyl and epoxide species.

EGO through the use of simulated annealing Monte Carlo simulations.[40]

Our statistical simulations based on the use of a simplistic energy scheme describing single-layer EGO showed that the aging process leads the oxygen functional groups on graphene to agglomerate. The arrested state at an arbitrary functionalization of graphene with epoxide or hydroxyl groups or both consists a nonhomogeneous phase of highly oxidized regions with average dimensions on the order of a nanometer surrounded by areas of pristine graphene (Figure 8). In this inhomogeneous phase, the aged EGO layer exhibits enhanced thermodynamic and kinetic stability.[40] In particular, within the highly oxidized domains, the oxygen functionalities are tightly packed and organized in an orderly fashion. High concentration, local order, and local spatial correlations of the oxygen functionalities have two major effects on the kinetic stability of EGO. First, the number of oxygen functionalities that are eligible to react according to the mechanisms shown in Figure 6 is about 20−30% of the total number of functionalities. Second, the eligible decomposition reactions become on average endothermic. Furthermore, DFT calculations also suggest that in the interior of highly oxidized domains of an aged EGO layer, the reaction energy barriers reach values larger than 1.6 eV (Figure 9). All these results underline that the origin of the kinetic stability of EGO lies in the formation of the inhomogeneous oxidation phase, wherein oxidized domains contain a high concentration of energetically stable and orderly, packed motifs of oxygen functional groups.

dx.doi.org/10.1021/ar400288h | *Acc. Chem. Res.* 2014, 47, 3331−3339

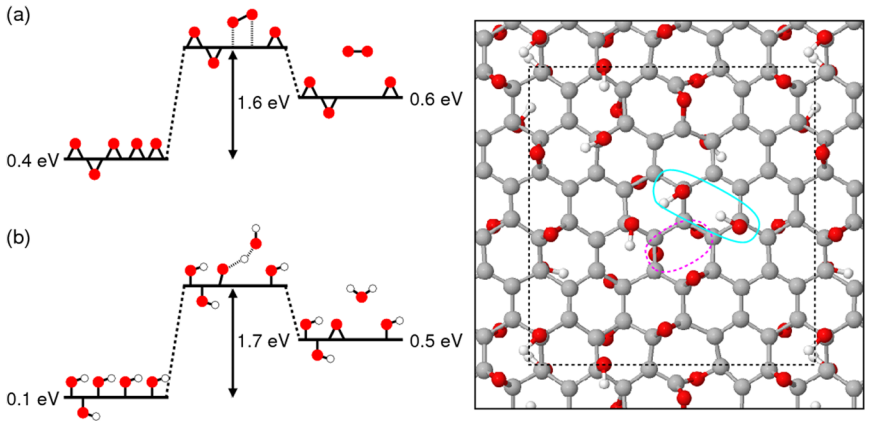

Figure 9. (a) Energy scheme for the reaction between epoxide groups in highly oxidized domains in aged EGO layers. Energy values of ΔG (per functional group) of reagents and products correspond to averages extracted from model structures of aged GO generated by using Monte Carlo simulations and the approximated energy scheme described in the text. The energy barrier of 1.6 eV is obtained from a NEB-DFT calculation using the model structure of GO shown on the right and the pair of reacting epoxide groups circled with the dashed magenta line. (b) Same as part a for the case of two hydroxyls embedded in a highly oxidized region of aged EGO layers. The energy barrier of 1.7 eV is obtained from NEB-DFT by considering the pair of reacting hydroxyl groups circled by the cyan line in the image on the right side.

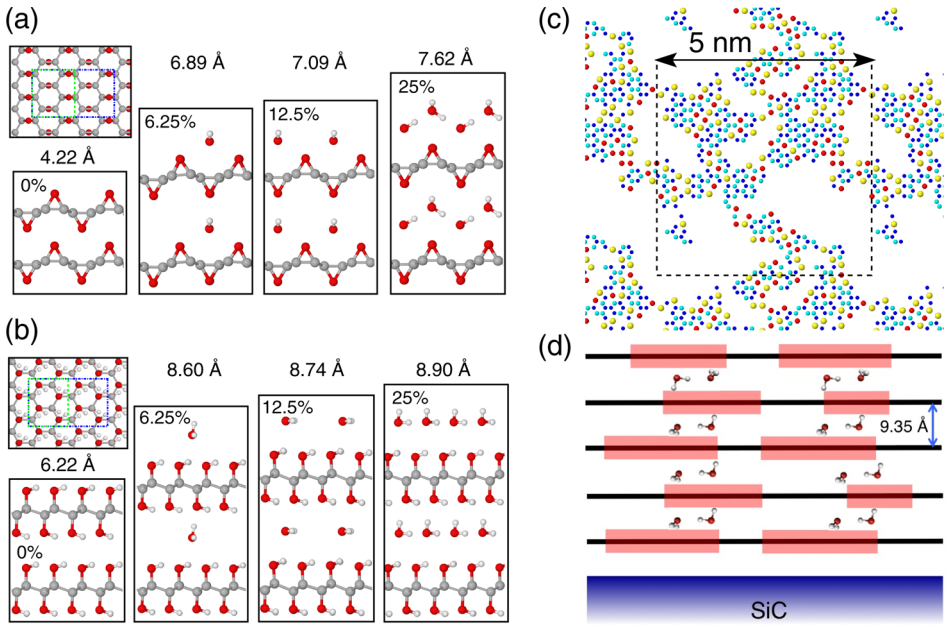

Figure 10. (a) EGO models used to mimic regions of the film where layers are fully oxidized with epoxide groups and trap an increasing concentration of water molecules. Colored rectangles in the top-left corner show the planar dimensions of the supercells used to model water concentrations of 6.25% (blue dash line) and 0%, 12.5%, and 25% (green dash line). (b) Same as part a with hydroxyl instead of epoxide species. (c) EGO layer presenting an inhomogeneous oxidation at the nanoscale of the carbon network (not shown) with epoxide (red and yellow colored balls) and hydroxyl (blue and cyan colored balls) chemisorbed on both sides of graphene (red and blue, one side; yellow and cyan, the opposite side). The model mimics the structure of a EGO film aged at room temperature; O/C ratio of 0.38, and fractions of hydroxyl and epoxide species equal to 0.27 and 0.11, respectively. (d) Schematic representation of a multilayer EGO film consisting of nonhomogeneously oxidized (red regions) and wetted graphene layers. The oxidized areas are rich in hydroxyl groups, while water molecules are trapped and pinch oxidized regions of neighboring layers.

5. INTERLAYER STRUCTURE OF EGO

XRD measurements show that the interlayer spacing in EGO is as large as 9.35 Å, and IR measurements also show that, in agreement with our XPS analyses, the water content in the aged oxide films does not exceed 10% of the total C. Experimental and computational studies of conventional GO suggest that a large interlayer spacing of about 10 Å can be reached only by incorporating significant amounts of water into the layered film, more than twice the quantity detected by IR and extrapolated from our XPS analysis of EGO. To elucidate these peculiar experimental observations, we need to account for all the results so far discussed.[25]

In Section 3, multilayer EGO was modeled using a stack of graphene layers hosting a homogeneous distribution of epoxide and hydroxyl species and incorporating a fraction of H_2O molecules up to 8%.[26,54] These types of model structures of EGO exhibit interlayer distances ranging between 4.5 and 6.5 Å, depending on the oxidation level, distribution of oxygen functional groups, and water content.[26,54] These results, in agreement with recent molecular dynamics studies of GO,[6,7] demonstrate that graphene oxide layers presenting O/C ratios

dx.doi.org/10.1021/ar400288h | Acc. Chem. Res. 2014, 47, 3331−3339

as high as 0.5 and exhibiting homogeneous distributions of oxygen functionalities on the carbon planes cannot explain the simultaneous occurrence of interlayer distances of 9.35 Å and water contents of 10%, as indicated by XRD and IR experiments of EGO.[25]

In Section 4,[40] we showed that epoxide and hydroxyl species chemisorbed on graphene are prone to agglomeration and that the aging process leads to the formation of EGO layers presenting at the nanoscale inhomogeneous oxidation (Figure 10).[40] To address the effect of an inhomogeneous oxidation phase on the interlayer separation in a multilayer EGO film, we considered model structures of EGO consisting of periodic stacks of graphene layers fully oxidized by either hydroxyl or epoxide groups, and including increasing concentrations of water molecules. For each model structure, we used DFT to perform a full structural optimization and determine the zero-temperature interlayer spacing.[25]

Our calculations show that, at all water concentrations, graphene layers fully oxidized with epoxides exhibit a smaller interlayer spacing than layers fully oxidized with hydroxyl groups. In the former case, the interlayer spacing reaches a value of only 7.5 Å when the water content is 25%, while carbon sheets oxidized with hydroxyl groups attain separations of 8.6 Å when only 6.25% H_2O is intercalated between the layers. In both cases, the interlayer spacing in EGO models containing 6.25% H_2O is significantly larger than the interlayer spacing in the dry EGO models, and it increases little for increasing further the water concentration. Overall, our DFT calculations support the model structure of EGO sketched in Figure 10d.[25] The graphene oxide layers present an inhomogeneous oxidation at the nanoscale, consisting of highly oxidized areas rich in hydroxyl groups surrounded by nanodomains of pristine graphene. Based on this model, a few (<10%) water molecules trapped between highly oxidized regions of nearest neighbor layers would be sufficient to reach interlayer separations of ∼9 Å.

6. CONCLUDING REMARKS

We have shown that DFT-based modeling has the capability of not only interpreting but also projecting out from the experiment detailed chemical and structural information on complex materials such as EGO. In this particular case, our DFT studies have led to elucidation of the origin of the metastability of EGO, its chemical composition, its intralayer and interlayer structure, and the relationship between interlayer spacing, water content, and intralayer spatial distribution of oxygen functionalities. Our DFT studies have also led to the discovery that Hummers oxidation introduces into the EG films not only oxygen groups such as epoxide and hydroxyl species but also a non-negligible quantity of hydrogen species, most likely present in the form of C−H species. Epoxide, hydroxyl, and C−H species are mobile and reactive, and our DFT calculations also show that protons can be exchanged between nearest neighbors oxygen functional groups by overcoming energy barriers as low as 0.3 eV. The presence of reactive hydrogen species and protons in EGO, together with the tendency of oxygen functional groups to agglomerate, favor the occurrence of reactions and the internal generation of water molecules and lead to an oxide film rich in hydroxyl species and presenting inhomogeneous oxidation and a porous layered structure with a spacing of ∼10 Å. This phenomenological information gives indirect but also very useful insight on the synthesis process of EGO, hinting at possible routes to modify, improve, control, and ultimately understand the Hummers method described in Section 2. A first step in this direction might be identifying what is the hydrogen source and at which stage of the synthesis process hydrogen incorporates into the EG film. Such knowledge would allow one to vary the quantity of excess hydrogen present in the as-synthesized films and thereby changing metastable behavior and possibly also final structure of the aged multilayer films. These studies would lead progressively to important information about the oxidation mechanisms converting the graphene film to EGO. It is also to be noted that our studies show that the structure of as-synthesized and aged films are significantly different: the aged films exhibit a porous structure and regions of pristine graphene, while the as-synthesized films are likely to exhibit homogeneous oxidation and an interlayer spacing up to 6−7 Å. This suggests that further Hummers oxidation of the aged films may lead to production of novel forms of graphene oxide, including O/C ratios larger than 0.5 and ordered distributions of epoxide and hydroxyl species. To conclude, novel understanding and control of complex materials such as graphene oxide are destined to arise from fullfilling the synergy between modeling, experimental characterization, and synthesis activities.

■ AUTHOR INFORMATION

Notes

The authors declare no competing financial interest.

Biographies

Si Zhou was born in 1986 in Benxi, China. She received her B.S. degree from the Nanjing University in 2009. Currently, she is a Ph.D. student in Angelo Bongiorno's group at Georgia Institute of Technology.

Angelo Bongiorno, Ph.D. in Physics, is currently Assistant Professor of Physics (and Chemistry and Biochemistry) at Georgia Institute of Technology. His computational research focuses on carbon and energy materials.

■ ACKNOWLEDGMENTS

The authors are thankful to Elisa Riedo, Claire Berger, Suenne Kim, Yike Hu, Walt de Heer, Carmela Aruta, Emiliano Di Gennaro, Cheng Gong, and Yves J. Chabal for the very useful discussions and for making available to us their experimental data. The authors also acknowledge the support of the National Science Foundation (NSF) Grants CMMI-1100290, DMR-0820382, and CHE-0946869.

■ REFERENCES

(1) Dreyer, D. R.; Park, S.; Bielawski, C. W.; Ruoff, R. S. The chemistry of graphene oxide. *Chem. Soc. Rev.* **2010**, *39*, 228−240.

(2) Wei, Z.; Wang, D.; Kim, S.; Kim, S.-Y.; Hu, Y.; Yakes, M. K.; Laracuente, A. R.; Dai, Z.; Marder, S. R.; Berger, C.; King, W. P.; de Heer, W. A.; Sheehan, P. E.; Riedo, E. Nanoscale tunable reduction of graphene oxide for graphene electronics. *Science* **2010**, *328*, 1373−1376.

(3) Eda, G.; Fanchini, G.; Chhowalla, M. Large-area ultrathin films of reduced graphene oxide as a transparent and flexible electronic material. *Nat. Nanotechnol.* **2008**, *3*, 270−274.

(4) Johari, P.; Shenoy, V. B. Modulating optical properties of graphene oxide: Role of prominent functional groups. *ACS Nano* **2011**, *5*, 7640−7647.

(5) Stoller, M. D.; Park, S. J.; Zhu, Y. W.; Ruoff, R. S. Graphene-based ultracapacitors. *Nano Lett.* **2008**, *8*, 3498−3502.

(6) Compton, O. C.; Cranford, S. W.; Putz, K. W.; An, Z.; Brinson, L. C.; Buehler, M. J.; Nguyen, S. T. Tuning the mechanical properties of graphene oxide paper and its associated polymer nanocomposites by controlling cooperative intersheet hydrogen bonding. *ACS Nano* **2012**, *6*, 2008−2019.
(7) Medhekar, N. V.; Ramasubramaniam, A.; Ruoff, R. S.; Shenoy, V. B. Hydrogen bond networks in graphene oxide composite paper: Structure and mechanical properties. *ACS Nano* **2010**, *4*, 2300−2306.
(8) Brodie, B. C. On the atomic weight of graphite. *Philos. Trans. R. Soc. London, Ser. A* **1859**, *149*, 249−259.
(9) Hummers, W. S.; Offeman, R. E. Preparation of graphitic oxide. *J. Am. Chem. Soc.* **1958**, *80*, 1339−1339.
(10) Marcano, D. C.; Kosynkin, D. V.; Berlin, J. M.; Sinitskii, A.; Sun, Z.; Slesarev, A.; Alemany, L. B.; Lu, W.; Tour, J. M. Improved synthesis of graphene oxide. *ACS Nano* **2010**, *4*, 4806−4814.
(11) Dimiev, A.; Kosynkin, D. V.; Alemany, L. B.; Chaguine, P.; Tour, J. M. Pristine graphite oxide. *J. Am. Chem. Soc.* **2012**, *134*, 2815−2822.
(12) Lerf, A.; He, H.; Forster, M.; Klinowski, J. Structure of graphite oxide revisited. *J. Phys. Chem. B* **1998**, *102*, 4477−4482.
(13) Hontoria-Lucas, C.; López-Peinado, A. J.; de D. López-González, J.; Rojas-Cervantes, M. L.; Martín-Aranda, R. M. Study of oxygen-containing groups in a series of graphite oxides: Physical and chemical characterization. *Carbon* **1995**, *33*, 1585−1592.
(14) Nakajima, T.; Matsuo, Y. Formation process and structure of graphite oxide. *Carbon* **1994**, *32*, 469−475.
(15) Casabianca, L. B.; Shaibat, M. A.; Cai, W. W.; Park, S.; Piner, R.; Ruoff, R. S.; Ishii, Y. NMR-based structural modeling of graphite oxide using multidimensional 13C solid-state NMR and ab initio chemical shift calculations. *J. Am. Chem. Soc.* **2010**, *132*, 5672−5676.
(16) Buchsteiner, A.; Lerf, A.; Pieper, J. Water dynamics in graphite oxide investigated with neutron scattering. *J. Phys. Chem. B* **2006**, *110*, 22328−22338.
(17) Acik, M.; Mattevi, C.; Gong, C.; Lee, G.; Cho, K.; Chhowalla, M.; Chabal, Y. J. The role of intercalated water in multilayered graphene oxide. *ACS Nano* **2010**, *4*, 5861−5868.
(18) Lerf, A.; Buchsteiner, A.; Pieper, J.; Schottl, S.; Dekany, I.; Szabo, T.; Boehm, H. P. Hydration behavior and dynamics of water molecules in graphite oxide. *J. Phys. Chem. Solids* **2006**, *67*, 1106−1110.
(19) Cerveny, S.; Barroso-Bujans, F.; Alegría, A.; Colmenero, J. Dynamics of water intercalated in graphite oxide. *J. Phys. Chem. C* **2010**, *114*, 2604−2612.
(20) Hossain, M. Z.; Johns, J. E.; Bevan, K. H.; Karmel, H. J.; Liang, Y. T.; Yoshimoto, S.; Mukai, K.; Koitaya, T.; Yoshinobu, J.; Kawai, M.; Lear, A. M.; Kesmodel, L. L.; Tait, S. L.; Hersam, M. C. Chemically homogeneous and thermally reversible oxidation of epitaxial graphene. *Nat. Chem.* **2012**, *4*, 305−309.
(21) Mattson, E. C.; Pu, H.; Cui, S.; Schofield, M. A.; Rhim, S.; Lu, G.; Nasse, M. J.; Ruoff, R. S.; Weinert, M.; Chen, M. G.-J. J.; Hirschmugl, C. J. Evidence of nanocrystalline semiconducting graphene monoxide during thermal reduction of graphene oxide in vacuum. *ACS Nano* **2011**, *5*, 9710−9717.
(22) Su, C. L.; Loh, K. P. Carbocatalysts: Graphene oxide and its derivatives. *Acc. Chem. Res.* **2013**, *46*, 2275−2285.
(23) Wan, X. J.; Huang, Y.; Chen, Y. S. Focusing on energy and optoelectronic applications: a journey for graphene and graphene oxide at large scale. *Acc. Chem. Res.* **2012**, *45*, 598−607.
(24) Park, S.; Lee, K.-S.; Bozoklu, G.; Cai, W.; Nguyen, S. T.; Ruoff, R. S. Graphene oxide papers modified by divalent ions—enhancing mechanical properties via chemical cross-linking. *ACS Nano* **2008**, *2*, 572−578.
(25) Zhou, S.; Kim, S.; Di Gennaro, E.; Hu, Y. K.; Gong, C.; Lu, X.; Berger, C.; de Heer, W.; Riedo, E.; Chabal, Y. J.; Aruta, C.; Bongiorno, A. Film structure of epitaxial graphene oxide on SiC: Insight on the relationship between interlayer spacing, water content, and intralayer structure. *Advanced Materials Interfaces* **2014**, DOI: 10.1002/admi.201300106.
(26) Kim, S.; Zhou, S.; Hu, Y. K.; Acik, M.; Chabal, Y. J.; Berger, C.; de Heer, W.; Bongiorno, A.; Riedo, E. Room-temperature metastability of multilayer graphene oxide films. *Nat. Mater.* **2012**, *11*, 544−549.
(27) Joshi, R. K.; Carbone, P.; Wang, F. C.; Kravets, V. G.; Su, Y.; Grigorieva, I. V.; Wu, H. A.; Geim, A. K.; Nair, R. R. Precise and ultrafast molecular sieving through graphene oxide membranes. *Science* **2014**, *343*, 752−754.
(28) Kim, H. W.; Yoon, H. W.; Yoon, S. M.; Yoo, B. M.; Ahn, B. K.; Cho, Y. H.; Shin, H. J.; Yang, H.; Paik, U.; Kwon, S.; Choi, J. Y.; Park, H. B. Selective gas transport through few-layered graphene and graphene oxide membranes. *Science* **2013**, *342*, 91−95.
(29) Li, H.; Song, Z. N.; Zhang, X. J.; Huang, Y.; Li, S. G.; Mao, Y. T.; Ploehn, H. J.; Bao, Y.; Yu, M. Ultrathin, molecular-sieving graphene oxide membranes for selective hydrogen separation. *Science* **2013**, *342*, 95−98.
(30) Boukhvalov, D. W.; Katsnelson, M. I. Modeling of graphite oxide. *J. Am. Chem. Soc.* **2008**, *130*, 10697−10701.
(31) Boukhvalov, D. W. Modeling of hydrogen and hydroxyl group migration on graphene. *Phys. Chem. Chem. Phys.* **2010**, *12*, 15367−15371.
(32) Boukhvalov, D. W. Modeling of epitaxial graphene functionalization. *Nanotechnology* **2011**, *22*, No. 055708.
(33) Yan, J.-A.; Chou, M. Y. Oxidation functional groups on graphene: structural and electronic properties. *Phys. Rev. B* **2010**, *82*, No. 125403.
(34) Yan, J.-A.; Xian, L.; Chou, M. Y. Structural and electronic properties of oxidized graphene. *Phys. Rev. Lett.* **2009**, *103*, No. 086802.
(35) Liu, L. Z.; Wang, L.; Gao, J. F.; Zhao, J. J.; Gao, X. F.; Chen, Z. F. Amorphous structural models for graphene oxides. *Carbon* **2012**, *50*, 1690−1698.
(36) Saxena, S.; Tyson, T. A.; Shukla, S.; Negusse, E.; Chen, H.; Bai, J. Investigation of structural and electronic properties of graphene oxide. *Appl. Phys. Lett.* **2011**, *99*, No. 013104.
(37) Xiang, H. J.; Wei, S.-H.; Gong, X. G. Structural motifs in oxidized graphene: A genetic algorithm study based on density functional theory. *Phys. Rev. B* **2010**, *82*, No. 035416.
(38) Zhang, W.; Carravetta, V.; Li, Z.; Luo, Y.; Yang, J. Oxidation states of graphene: Insights from computational spectroscopy. *J. Chem. Phys.* **2009**, *131*, No. 244505.
(39) Duong, D. L.; Kim, G.; Jeong, H. K.; Lee, Y. H. Breaking AB stacking order in graphite oxide: Ab initio approach. *Phys. Chem. Chem. Phys.* **2010**, *12*, 1595−1599.
(40) Zhou, S.; Bongiorno, A. Origin of the chemical and kinetic stability of graphene oxide. *Sci. Rep.* **2013**, *3*, No. 2484.
(41) Boukhvalov, D. W. DFT modeling of the covalent functionalization of graphene: From ideal to realistic models. *RSC Adv.* **2013**, *3*, 7150−7159.
(42) Wang, L.; Sun, Y. Y.; Lee, K.; West, D.; Chen, Z. F.; Zhao, J. J.; Zhang, S. B. Stability of graphene oxide phases from first-principles calculations. *Phys. Rev. B* **2010**, *82*, No. 161406.
(43) Paci, J. T.; Belytschko, T.; Schatz, G. C. Computational studies of the structure, behavior upon heating, and mechanical properties of graphite oxide. *J. Phys. Chem. C* **2007**, *111*, 18099−18111.
(44) Boukhvalov, D. W.; Son, Y. W. Oxygen reduction reactions on pure and nitrogen-doped graphene: a first-principles modeling. *Nanoscale* **2012**, *4*, 417−420.
(45) Carlsson, J. M.; Hanke, F.; Linic, S.; Scheffler, M. Two-Step Mechanism for Low-Temperature Oxidation of Vacancies in Graphene. *Phys. Rev. Lett.* **2009**, *102*, No. 166104.
(46) Nguyen, M. T.; Erni, R.; Passerone, D. Two-dimensional nucleation and growth mechanism explaining graphene oxide structures. *Phys. Rev. B* **2012**, *86*, No. 115406.
(47) Boukhvalov, D. W.; Son, Y. W. Covalent functionalization of strained graphene. *ChemPhysChem* **2012**, *13*, 1463−1469.
(48) Larciprete, R.; Fabris, S.; Sun, T.; P. Lacovig, A. B.; Lizzit, S. Dual path mechanism in the thermal reduction of Graphene oxide. *J. Am. Chem. Soc.* **2011**, *133*, 17315−17321.

(49) Bagri, A.; Mattevi, C.; Acik, M.; Chabal, Y. J.; Chhowalla, M.; Shenoy, V. B. Structural evolution during the reduction of chemically derived graphene oxide. *Nat. Chem.* **2010**, *2*, 581−587.
(50) Gao, W.; Alemany, L. B.; Ci, L.; Ajayan, P. M. New insights into the structure and reduction of graphite oxide. *Nat. Chem.* **2009**, *1*, 403−408.
(51) Lu, N.; Huang, Y.; Li, H. B.; Li, Z. Y.; Yang, J. L. First principles nuclear magnetic resonance signatures of graphene oxide. *J. Chem. Phys.* **2010**, *133*, No. 034502.
(52) Acik, M.; Lee, G.; Mattevi, C.; Chhowalla, M.; Cho, K.; Chabal, Y. J. Unusual infrared-absorption mechanism in thermally reduced graphene oxide. *Nat. Mater.* **2010**, *9*, 840−845.
(53) Nair, R. R.; Wu, H. A.; Jayaram, P. N.; Grigorieva, I. V.; Geim, A. K. Unimpeded permeation of water through helium-leak-tight graphene-based membranes. *Science* **2012**, *335*, 442−444.
(54) Zhou, S.; Kim, S.; Bongiorno, A. Chemical structure of oxidized multilayer epitaxial graphene: A density functional theory study. *J. Phys. Chem. C* **2013**, *117*, 6267−6274.
(55) Giannozzi, P.; Baroni, S.; Bonini, N.; Calandra, M.; Car, R.; Cavazzoni, C.; Ceresoli, D.; Chiarotti, G. L.; Cococcioni, M.; Dabo, I.; Da1 Corso, A.; de Gironcoli, S.; Fabris, S.; Fratesi, G.; Gebauer, R.; Gerstmann, U.; Gougoussis, C.; Kokalj, A.; Lazzeri, M.; Martin-Samos, L.; Marzari, N.; Mauri, F.; Mazzarello, R.; Paolini, S.; Pasquarello, A.; Paulatto, L.; Sbraccia, C.; Scandolo, S.; Sclauzero, G.; Seitsonen, A. P.; Smogunov, A.; Umari, P.; Wentzcovitch, R. M. QUANTUM ESPRESSO: A modular and open-source software project for quantum simulations of materials. *J. Phys.: Condens. Matter* **2009**, *21*, No. 395502.
(56) Perdew, J. P.; Burke, K.; Ernzerhof, M. Generalized gradient approximation made simple. *Phys. Rev. Lett.* **1996**, *77*, 3865−3868.
(57) Grimme, S. Semiempirical GGA-type density functional constructed with a long-range dispersion correction. *J. Comput. Chem.* **2006**, *27*, 1787−1799.
(58) Ren, P. G.; Yan, D. X.; Ji, X.; Chen, T.; Li, Z. M. Temperature dependence of graphene oxide reduced by hydrazine hydrate. *Nanotechnology* **2011**, *22*, No. 055705.
(59) Galande, C.; Mohite, A. D.; Naumov, A. V.; Gao, W.; Ci, L. J.; Ajayan, A.; Gao, H.; Srivastava, A.; Weisman, R. B.; Ajayan, P. M. Quasi-Molecular Fluorescence from Graphene Oxide. *Sci. Rep.* **2011**, *1*, No. 85.